Adaptive Normalised Matched Filter Performance in Medium Grazing Angle Sea Clutter

Michael McDonald
Defence Research & Development Canada (DRDC)
Ottawa, Canada
Mike.Mcdonald@drdc-rddc.gc.ca

Delphine Cerutti-Maori
Fraunhofer FHR
Wachtberg, Germany
Delphine.Cerutti-Maori@fhr.fraunhofer.de

***Abstract*—The detection performance of the adaptive normalised matched filter (ANMF) detector structure is assessed against real multi-channel, medium grazing angle, radar sea clutter data processed via space-time adaptive processing (STAP). Significant departures from constant false alarm rate (CFAR) performance are observed and linked to discrepancies between the assumed form of the spherically invariant random process (SIRP) which is used to derive the ANMF detection statistics and the actual form of the stochastic model representing the real world clutter characteristics.**

***Index Terms*—Radar, GMTI, Maritime surveillance, Sea clutter analysis, STAP.**

I. Introduction

Traditional noncoherent maritime detection performance under high grazing angle (HGA) and medium grazing angle (MGA) surveillance geometries is expected to be severely degraded due to the large increases in clutter cross-section that are associated with these steep geometries. A promising approach to aid in mitigating the anticipated performance degradation is the application of coherent processing techniques. This paper examines the effectiveness of sub-optimal STAP processing techniques for maritime surface target surveillance. In the following we examine the application of post-Doppler STAP utilizing covariance matrix estimations via local range samples and process real sea clutter data with simulated embedded targets. A post-Doppler ANMF detector structure is derived per an assumption of spherically invariant random process (SIRP) clutter statistics and the resulting constant false alarm rate (CFAR) and probability of detection (PD) performance are evaluated for medium grazing angle sea clutter. Departures of the ANMF from ideal performance are examined and related to limitations of the statistical clutter model assumed during its derivation.

II. Data collection

The data underlying this analysis was acquired using the Fraunhofer FHR PAMIR system operating in a scan-MTI mode in a sidelooking configuration [1], [2]. During the collection trial the radar platform flew at an altitude of 2500 m (8200 feet) with a velocity of 100 m/s. The antenna grazing angle was approximately 20°. Two data collection passes (see Figure 1) were undertaken with look directions corresponding to approximately downwind (pass 1) and upwind (pass 2) geometries, i.e., wind is blowing away from or towards the radar antenna pointing direction, respectively. The trial took place in the North Sea between Helgoland and Wilhelmshaven in Germany in December, 2009. Key operating parameters and collection geometry details are provided in Table I. Sea conditions were moderate with a reported swell height of 0.9-1.5 m and a wind sea wave height of 0.4-0.5 m.

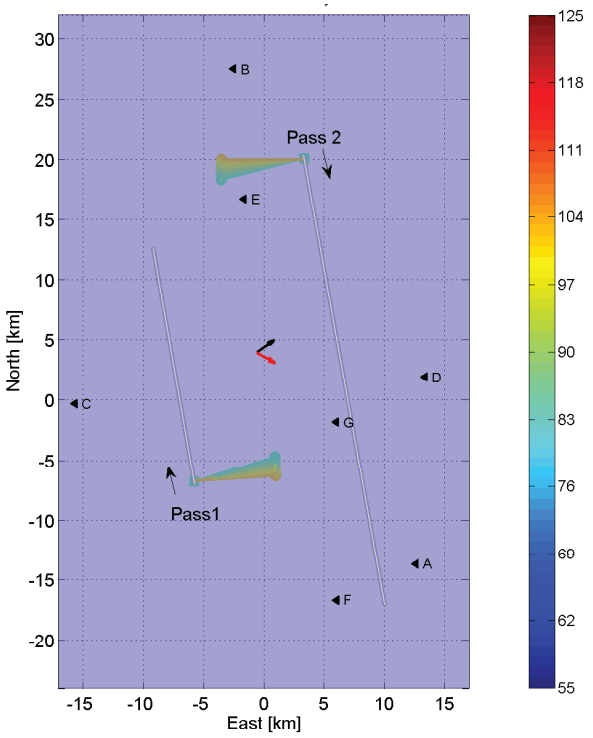

Fig. 1. Flight geometries in the East-North-Up coordinate system. Wind direction and swell direction are indicated by the black and the red arrows, respectively. The color codes the steering direction [°] of the antenna.

III. SIRP model and post-Doppler ANMF formulation

As discussed above, STAP offers the potential to improve the overall detection at HGA through its ability to temporally and spatially separate clutter and target signals. The topic of STAP has been extensively addressed in the literature and a detailed description of the STAP algorithms is beyond the

978-1-4673-9655-4/15/$31.00

TABLE I
OPERATING PARAMETERS AND COLLECTION GEOMETRY FOR PAMIR DATA SET

Mean range from aircraft to target	7.3 km
Viewing geometry	Sidelooking looking wrt aircraft motion
Aircraft altitude	2500 m (8200')
Grazing angle	20^o
Platform velocity	100 m/s
Range resolution	7.5 m
Transmit frequency	9.09 & 9.50 GHz
Antenna azimuth	80 cm
Number of channels	3
Antenna phase centre separation	26.6 cm
Antenna TX & RX polarisation	V-V
Coherent processing interval (CPI)	42.6 ms
Effective pulse repetition frequency (PRF)	3 kHz
Centre point of the data take	(53.98 N, 7.91 E)

scope of the current paper. The interested reader is referred to Ward [3] for an excellent overview of the topic. A well recognised challenge to the successful implementation of fully adaptive STAP is the large dimensionality of the measurement vectors and the correspondingly large covariance matrix size. For example, the data examined in this paper produces a measurement vector with a dimension of $Q = 192$ (number of apertures times number of pulses in a CPI) leading to a covariance matrix with $Q \times Q$ dimensionality. The computational load associated with the inversion of matrices of this size is significant and, in addition, a large number of background samples is required to achieve accurate estimates [4]. These dimensionality issues have long been recognised within the ground moving target indication (GMTI) community and it is common to employ partially adaptive approaches which reduce the dimensionality of the adaptation problem. In particular, PRI staggered post-Doppler (PSPD) partially adaptive STAP was chosen as the baseline sub-optimal STAP processing algorithm used in this paper. PSPD results in significant reductions in the rank of the estimated covariance matrices and is dependent on the assumption of statistical independence of clutter signal between frequency bins after conversion to the frequency domain as will be clarified below [3].

The ANMF detection statistic derivation is commonly developed from the assumption that clutter measurements are well represented as spherically invariant random variables (SIRVs), i.e., from a SIRP. The SIRP has frequently been proposed as a tractable statistical characterisation of the complex envelope of the sea clutter radar echo returns and takes the form

$$p(\mathbf{z}) = \int_0^\infty \frac{1}{\pi^Q |\tau \mathbf{M}|} e^{-\frac{\mathbf{z}^\dagger \mathbf{M}^{-1} \mathbf{z}}{\tau}} p_{\boldsymbol{\tau}}(\tau) \mathrm{d}\tau, \tag{1}$$

where $\mathbf{M}$ denotes the normalized covariance matrix and Q is the length of the complex space-time measurement vector $\mathbf{z}$. The variable τ models the power or texture which has a distribution given by $p_{\boldsymbol{\tau}}(\tau)$ [5], [6].

The presence of the integral in equation (1) is problematic and leads to an expression for the likelihood ratio which cannot be efficiently evaluated. The ANMF detector is a suboptimal approximation which eliminates the need to evaluate the integral by treating the random variable τ as an unknown deterministic variable for which a maximum likelihood (ML) estimates $\hat{\tau}$ is calculated. Upon making this substitution we can form the ANMF detection statistic as follows

$$\Lambda_{\text{ANMF}} = \frac{|\mathbf{p}^\dagger \mathbf{M}^{-1} \mathbf{z}|^2}{(\mathbf{p}^\dagger \mathbf{M}^{-1} \mathbf{p})(\mathbf{z}^\dagger \mathbf{M}^{-1} \mathbf{z})}. \tag{2}$$

where $\mathbf{p}$ represents the steering vector corresponding to the postulated target signal. To better understand some of the implicit assumptions underlying the SIRP and the resulting ANMF, it is useful to explicitly derive the frequency domain representation of the ANMF. Without loss of generality, the data vector $\mathbf{z}$ can be expressed equivalently in the frequency domain as

$$\mathbf{z}_f = [\mathbf{z}_{f_1}^{\mathrm{T}}, \mathbf{z}_{f_2}^{\mathrm{T}}, \cdots, \mathbf{z}_{f_N}^{\mathrm{T}}]^{\mathrm{T}} \tag{3}$$

where f_i corresponds to a given frequency component and N is the number of temporal samples. For the case of a single channel system, the $\mathbf{z}_{f_i}$ components become scalar and the formulation is analogous to that presented by Conte et al. [7].

Under the SIRP model, we can recast $\mathbf{z}$ as

$$\mathbf{z} = \sqrt{\tau}\mathbf{x} \tag{4}$$

where $\mathbf{x}$ is a zero mean complex Gaussian (CN) process. $\mathbf{z}_f$ now becomes

$$\mathbf{z}_f = \sqrt{\tau}[\mathbf{x}_{f_1}, \mathbf{x}_{f_2}, \cdots, \mathbf{x}_{f_N}]^{\mathrm{T}} = \sqrt{\tau}\mathbf{x}_f \tag{5}$$

and

$$\mathbf{R}_f = \mathcal{E}\{\mathbf{z}_f \mathbf{z}_f^\dagger\} = \tau \mathcal{E}\{\mathbf{x}_f \mathbf{x}_f^\dagger\} = \tau \mathbf{M}_f. \tag{6}$$

To arrive at a formulation compatible with the PSPD STAP we now assume that the frequency components $\mathbf{x}_{f_i}$ are statistically independent. The normalized covariance matrix then takes the form of a block diagonal matrix

$$\mathbf{R}_f = \tau \begin{bmatrix} \mathbf{M}_{f_1} & \mathbf{0} & \cdots & \mathbf{0} \\ \mathbf{0} & \mathbf{M}_{f_2} & \mathbf{0} & \vdots \\ \vdots & \mathbf{0} & \ddots & \mathbf{0} \\ \mathbf{0} & \cdots & \mathbf{0} & \mathbf{M}_{f_N} \end{bmatrix} \tag{7}$$

where $\mathbf{M}_{f_i} = \mathcal{E}\{\mathbf{x}_{f_i} \mathbf{x}_{f_i}^\dagger\}$.

The assumption of frequency independence is only approximately valid as cross-terms between frequency terms of the sample covariance matrices are observed to be suppressed by 10-15 dB but the assumption proves useful in practice due to the easing of the sample support requirements and computational costs associated with the inversion of a high rank covariance matrices. Given the well known effect of Doppler broadening due to aircraft motion one can anticipate that Doppler bins which are reasonably well separated in frequency will correspond to different azimuth locations on the sea surface and will exhibit some degree of statistical independence.

For typical target scenarios, the target steering vector is assumed to be well modelled by a single target frequency. The corresponding steering vector for a target with Doppler frequency f_i is then given by

$$\mathbf{p}_f = [\mathbf{0}^{\mathrm{T}} \cdots \mathbf{0}^{\mathrm{T}}\, \mathbf{p}_{f_i}^{\mathrm{T}}\, \mathbf{0}^{\mathrm{T}} \cdots \mathbf{0}^{\mathrm{T}}]^{\mathrm{T}} \tag{8}$$

where $\mathbf{0}$ is a vector of zeros and $\mathbf{p}_{f_i}$ is the space-time steering vector for the considered Doppler frequency f_i and desired look direction.

Under the assumption of frequency independence, we can now rewrite (2) in the frequency domain as

$$\begin{aligned}\Lambda_{\mathrm{ANMF}_{f_i}} &= \frac{|\mathbf{p}_f^{\dagger}\mathbf{M}_f^{-1}\mathbf{z}_f|^2}{(\mathbf{p}_f^{\dagger}\mathbf{M}_f^{-1}\mathbf{p}_f)(\mathbf{z}_f^{\dagger}\mathbf{M}_f^{-1}\mathbf{z}_f)} \\ &= \frac{|\mathbf{p}_{f_i}^{\dagger}\mathbf{M}_{f_i}^{-1}\mathbf{z}_{f_i}|^2}{(\mathbf{p}_{f_i}^{\dagger}\mathbf{M}_{f_i}^{-1}\mathbf{p}_{f_i})(\sum_{j=1}^{N}\mathbf{z}_{f_j}^{\dagger}\mathbf{M}_{f_j}^{-1}\mathbf{z}_{f_j})}.\end{aligned} \tag{9}$$

In this paper the iterative approach of equation (7) of Conte et al. [8] was used to calculate the normalized sample covariance matrix. The frequency domain formulation of the iterative approach is therefore given as

1) Form initial estimate of $\mathbf{M}_f$ over K range cells

$$\begin{aligned}\widehat{\mathbf{M}}_f^{\mathrm{t}} &= \frac{1}{QK}\sum_{k=1}^{K}\frac{\mathbf{z}_f(k)\mathbf{z}_f^{\dagger}(k)}{\mathbf{z}_f^{\dagger}(k)\mathbf{z}_f(k)} \\ &= \frac{1}{QK}\sum_{k=1}^{K}\begin{bmatrix} \frac{\mathbf{z}_{f_1}(k)\mathbf{z}_{f_1}^{\dagger}(k)}{\sum_{j=1}^{N}\mathbf{z}_{f_j}^{\dagger}(k)\mathbf{z}_{f_j}(k)} & \mathbf{0} & \mathbf{0} \\ \mathbf{0} & \ddots & \mathbf{0} \\ \mathbf{0} & \mathbf{0} & \frac{\mathbf{z}_{f_N}(k)\mathbf{z}_{f_N}^{\dagger}(k)}{\sum_{j=1}^{N}\mathbf{z}_{f_j}^{\dagger}(k)\mathbf{z}_{f_j}(k)} \end{bmatrix} \\ &= \frac{1}{QK}\sum_{k=1}^{K}\begin{bmatrix} \widehat{\mathbf{M}}_{f_1}^{\mathrm{t}} & \mathbf{0} & \cdots & \mathbf{0} \\ \mathbf{0} & \widehat{\mathbf{M}}_{f_2}^{\mathrm{t}} & \mathbf{0} & \vdots \\ \vdots & \mathbf{0} & \ddots & \mathbf{0} \\ \mathbf{0} & \cdots & \mathbf{0} & \widehat{\mathbf{M}}_{f_N}^{\mathrm{t}} \end{bmatrix}\end{aligned} \tag{10}$$

2) Form an estimate of the underlying power $\hat{\tau}^{\mathrm{t}}(k)$ for each range sample k

$$\hat{\tau}^{\mathrm{t}}(k) = \sum_{j=1}^{N}\frac{\mathbf{z}_{f_j}^{\dagger}(k)(\widehat{\mathbf{M}}_{f_j}^{\mathrm{t}})^{-1}\mathbf{z}_{f_j}(k)}{Q} \tag{11}$$

3) Form new estimate of $\widehat{\mathbf{M}}_{f_i}$

$$\widehat{\mathbf{M}}_{f_i}^{\mathrm{t+1}} = \frac{1}{QK}\sum_{k=1}^{K}\frac{\mathbf{z}_{f_i}(k)\mathbf{z}_{f_i}^{\dagger}(k)}{\hat{\tau}^{\mathrm{t}}(k)} \tag{12}$$

4) Repeat from step 2

It is important to note that the traces of the subcomponent diagonal block matrices,$\widehat{\mathbf{M}}_{f_i}^{\mathrm{t+1}}$, comprising $\mathbf{R}_f$ are not of equal amplitude. This latter point is easily observed in equation (12) where the trace of each $\widehat{\mathbf{M}}_{f_i}^{\mathrm{t+1}}$ is seen to be proportional to the mean power of the corresponding Doppler bin divided by overall estimate of $\hat{\tau}$. The form of equations (5) and (6) further highlights the fact that the SIRP formulation implicitly assumes that all frequency components of $\mathbf{z}_f$ are equivalently scaled by parameter τ. With this interpretation in mind, it is observed that the summation term in the denominator of equation (9) represents the summation of values of τ independently estimated using each Doppler bin. The formulation of the ANMF detector is compatible with the presence of a clutter component with the total spectral power modulated per the distribution $p_{\boldsymbol{\tau}}(\tau)$. In contrast, previous spectral and stochastic modelling of the PAMIR data set in question [9] has shown that the underlying clutter is in fact poorly modelled by single component clutter with much better modelling accuracy obtained through the assumption of two independent K-distributed clutter components. It is anticipated that mismatches between the SIRP assumption and the actual clutter characteristics will result in degraded ANMF performance. To assess this potential degradation, the CFAR and detection performance of the ANMF detector are evaluated in the next section using the PAMIR data.

IV. ANMF PERFORMANCE

Figure 2 summarizes the CFAR performance achieved through application of the post-Doppler ANMF detector to the PAMIR data. The top panel presents the actual probability of false alarm (PFA) achieved versus Doppler velocity when the detection threshold is set to the theoretical level required to achieve a desired $PFA = 10^{-3}$ under the assumption of a true SIRP. The bottom panel presents the corresponding results for a desired $PFA = 10^{-4}$. We first examine the results for the case where the summation in the denominator of equation (9) is assumed to span all frequency bins, i.e., $N = 64$ for this data set. Under this condition the frequency domain ANMF processing corresponds exactly to the commonly reported time domain formulation where it has been assumed that frequency components $\mathbf{z}_f$ are independent.

It is readily apparent from the actual measured performance that the desired CFAR versus Doppler velocity characteristic is not achieved and that a significant increase of the PFA beyond the desired setting is observed across much of the endoclutter region. Upon further consideration it should be apparent that the formulation of equation (9) corresponds to a pure clutter case and does not account for receiver noise. Gini et al. [10] previously examined the simpler case of a two-component model comprised of K-distributed and

Rayleigh components and showed that optimal detector structure required the evaluation of an integral over the pdf of the underlying texture component. The form of equation (9) suggests that one approach to minimize this effect would be to limit the summation range to Doppler bins in which the clutter to noise ratio was very large. Furthermore, if one restricts the summation to a range of Doppler local in frequency to the Doppler bin under test (DUT), then the SIRP requirement that $p_{\boldsymbol{\tau}}(\tau)$ values be fully correlated across all Doppler bins can now be relaxed to the condition that $p_{\boldsymbol{\tau}}(\tau)$ is correlated across the reduced summation range.

Results are also presented in Figure 2 for the cases when the summation is restricted to $N = 1, 3$ and 9. For the $N = 1$ case, only the DUT is used for the estimation of $p_{\boldsymbol{\tau}}(\tau)$. This can be seen to have implications with regards to probability of detection of targets and is discussed further below. For the entire endoclutter band extending from from -3 m/s to 6 m/s, the CFAR performance for the $N = 9$ and $N = 64$ case is worse than that obtained using the narrower Doppler summations. This observation highlights the fact that the underlying clutter is not well represented by a SIRP. Per the discussion on receiver noise above, this result was anticipated for the $N = 64$ result, but the effect would have been expected to be negligible for the $N = 9$ case for DUTs with high CNR.

The behaviour of the $N = 1$ and $N = 3$ results is more nuanced. Attempts to explain the measured variations of both effective shape parameter and spectral power variation versus Doppler frequency led to the fitting of a two component clutter mode to the data in question [9]. These fitting efforts indicated the the variation in both statistics and spectral power versus Doppler frequency could not be explained using a single component fit, even it were allowed to possess a bimodal spectral shape, and it was necessary to fit at least two statistically independent clutter components to obtain a good fit. We note that the velocity band -5 to 3 m/s corresponds to spectral region dominated by Bragg scattering while the fast scatter (FS) component was shown to dominate in the velocity band corresponding to 3 to 6 m/s. Upon careful examination of the $N = 1$ and $N = 3$ results in Figure 2 we observe that the relative performance of these formulations is in fact different depending on whether we are examining a Bragg or FS dominant region. In the FS dominated region the CFAR performance of the N=1 and N=3 detectors is seen to be virtually identical while in the Bragg dominated region the $N = 1$ CFAR performance is superior to the $N = 3$ results. This dependency on the Doppler bin summation length has not been previously reported and is informative as it further supports the assertion that the character of the FS versus Bragg clutter is fundamentally different in more than just mean Doppler frequency, i.e., it supports the assertion that clutter response arises from a (at least) two-component clutter model which is at odds with the SIRP assumption. More specifically it suggests that the FS texture parameter is partially correlated across at least 3 Doppler bins while the Bragg is not.

The above results have implications for the practical implementation of detection strategies. While the $N = 1$ formulation appears to offer universally superior or equal CFAR performance across the endoclutter region, it is important to recall that this formulation uses only the DUT to estimate the current value of τ. Since we do not know a priori if a target is present in the DUT, we can anticipate that calculation of the $N = 1$ denominator term, $\mathbf{z}_{f_i}^{\dagger}\mathbf{M}_{f_j}^{-1}\mathbf{z}_{f_i}$, will result in some level of self-suppression when a target is present. If the target can be assumed to present a highly coherent (i.e. narrow spectrum confined to one Doppler bin) signal for any given CPI, then this self-suppression effect will be reduced when a larger Doppler summation range is used. To examine this effect we plot the PD versus Doppler velocity for a range of signal-to-noise ratio (SNR) values in Figure 3. The PD results are seen to be consistent with the discussion above with $N = 3$ providing the best overall detection performance. Therefore we have a condition in which the best detector formulation may vary between different velocity bands within the endoclutter region. Throughout the FS region the $N = 3$ formulation provides superior PD performance to the $N = 1$ while both cases provide equivalent CFAR performance. This suggests that the $N = 3$ formulation should be used throughout the FS dominated velocity band. In contrast, for the Bragg dominated region the $N = 1$ formulation provides superior CFAR performance while the $N = 3$ formulation provides the best PD. Whereas the choice of detector formulation is clear for FS dominant region, the Bragg region requires a careful consideration of tradeoffs.

As discussed above, the proposed combination of clutter mechanisms responsible for the observed clutter returns appear to be most consistent with models in which two (or possibly more) independent physical mechanisms are assumed to be present. This model is not consistent with the SIRP formulation. Based on these observations one might therefore be

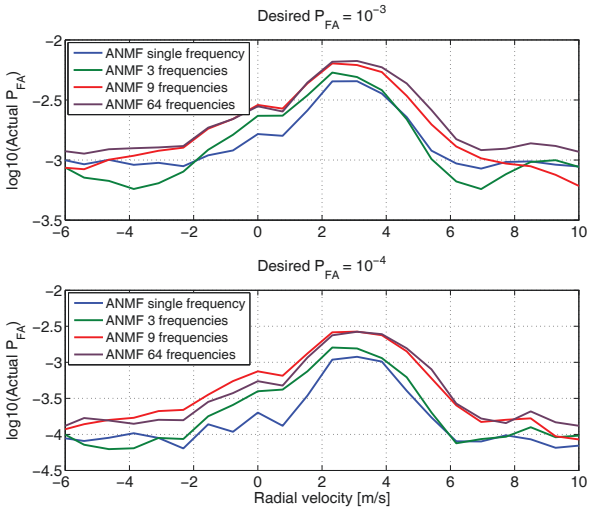

Fig. 2. Actual PFA achieved versus Doppler velocity for ANMF detection with $\mathbf{z}_f^{\dagger}\mathbf{M}_f^{-1}\mathbf{z}_f$ summation lengths of 1, 3, 9 and 64 frequency bins. Threshold set to achieve PFA=10^{-3} and PFA=10^{-4} for SIRP clutter statistics. Upwind viewing geometry.

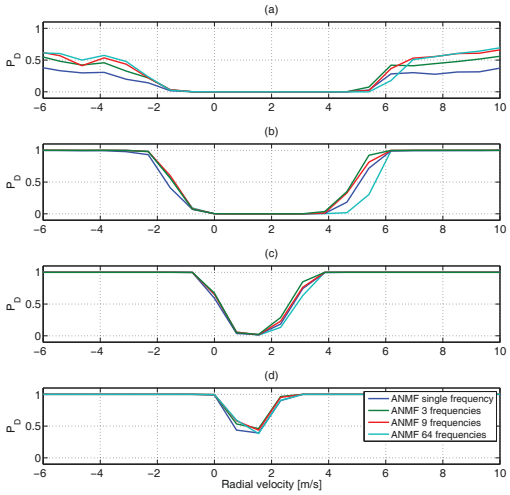

Fig. 3. Probability of detection for PFA=10^{-4}. SNR range is (a) 7 dB, (b) 13 dB, (c) 25 dB and (d) 31 dB.

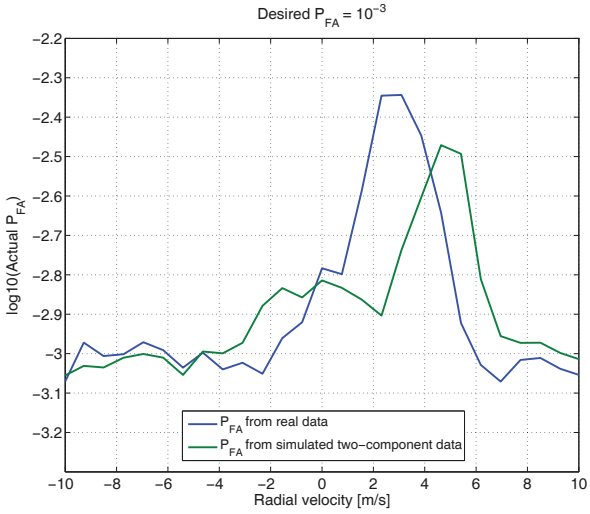

Fig. 4. Measured PFA output from ANMF detector with threshold set to achieve PFA=10^{-3}. Blue curve corresponds to performance against real PAMIR data. Green curve corresponds to performance against simulated data using equation (13).

tempted to assume that the clutter could be simply modelled as two-component formulation comprised of two K-distributed features as follows

$$p(\mathbf{z}) = \iint_0^\infty \frac{1}{\pi^Q |\tau_B \mathbf{M_B} + \tau_{FS} \mathbf{M_{FS}}|} p_{\boldsymbol{\tau}_\mathbf{B}}(\tau_B) p_{\boldsymbol{\tau}_\mathbf{FS}}(\tau_{FS}) \\ e^{-\ \mathbf{z}^\dagger (\tau_B \mathbf{M_B} + \tau_{FS} \mathbf{M_{FS}})^{-1} \mathbf{z}} \mathrm{d}\tau_B \mathrm{d}\tau_{FS}, \tag{13}$$

where $\mathbf{M_B}$ and $\mathbf{M_{FS}}$ correspond to the Bragg and FS covariance matrices and τ_B and τ_{FS} are the Bragg and FS texture values with distributions $p_{\boldsymbol{\tau}_\mathbf{B}}(\tau_B)$ and $p_{\boldsymbol{\tau}_\mathbf{FS}}(\tau_{FS})$, respectively. In this formulation each component is assumed to correspond to a separate SIRP. There is currently no ANMF analogous detector derivation for this two-component model. As a preliminary test of the proposed model we generated simulated data consistent with equation (13) before detecting via the ANMF detector structure so as to measure the resulting performance. Figure 4 summarises the measured CFAR response for the real PAMIR data and simulated data with parameters set per the previous modelling activity. The two responses are seen to be poorly aligned with the peak PAMIR PFA mismatch occurring at approximately 3 m/s and the peak simulated PFA mismatch occurring at approximately 4.6 m/s. Clearly the proposed two-component model, while capable of producing a good match to raw clutter statistics, fails to capture some phenomenological characteristic of the real sea clutter which directly impacts on the resulting ANMF CFAR performance. Future work will be undertaken to develop a more representative two-component formulation.

V. Conclusions

A frequency domain formulation of the ANMF detector compatible with post-Doppler STAP processing was developed and shown to provide advantages due to the relaxation of the requirement for the texture scaling factor, τ, to be fully correlated across all bins. Detection performance was assessed for a range of different assumptions with regards to the frequency span over which τ could be assumed correlated. Two different regimes were identified in which τ correlation frequency span could be seen to differ leading to different formulations for the best performing detector.

Acknowledgement

Thanks is extended to all members of the NATO SET 185 Technical Group whose feedback and insights assisted greatly in the development of the results presented in this paper.

References

[1] D. Cerutti-Maori, J. Klare, A. R. Brenner, and J. H. G. Ender, "Wide area traffic monitoring with the sar/gmti system pamir," IEEE Transactions on Geoscience and Remote Sensing, vol. 46, no. 10, pp. 3019–3030, October 2008.

[2] M. Mcdonald, D. Cerutti-Maori, and A. Damini, "Characterisation and cancellation of medium grazing angle sea clutter," in Radar Conference (EuRAD), 2010 European, 2010, pp. 172–175.

[3] J. Ward, "Space-time adaptive processing for airborne radar," Lincoln Laboratory, MIT, Technical report 1015, December 1994.

[4] I. Reed, J. Mallett, and L. Brennan, "Rapid convergence rate in adaptive arrays," Aerospace and Electronic Systems, IEEE Transactions on, vol. AES-10, no. 6, pp. 853–863, 1974.

[5] E. Conte and M. Longo, "Characterisation of radar clutter as a spherically invariant random process," Communications, Radar and Signal Processing, IEE Proceedings F, vol. 134, no. 2, pp. 191–197, 1987.

[6] M. Rangaswamy, D. Weiner, and A. Ozturk, "Non-gaussian random vector identification using spherically invariant random processes," Aerospace and Electronic Systems, IEEE Transactions on, vol. 29, no. 1, pp. 111–124, 1993.

[7] E. Conte, M. Lops, and G. Ricci, "Adaptive detection schemes in compound-gaussian clutter," Aerospace and Electronic Systems, IEEE Transactions on, vol. 34, no. 4, pp. 1058–1069, 1998.

[8] E. Conte, A. De Maio, and G. Ricci, "Recursive estimation of the covariance matrix of a compound-gaussian process and its application to adaptive cfar detection," Signal Processing, IEEE Transactions on, vol. 50, no. 8, pp. 1908–1915, 2002.

[9] M. McDonald and D.Cerutti-Maori, "Statistical and spectral modelling of medium grazing angle coherent radar data," in submitted to 2015 IEEE Radar Conference.

[10] F. Gini, M. Greco, A. Farina, and P. Lombardo, "Optimum and mismatched detection against k-distributed plus gaussian clutter," Aerospace and Electronic Systems, IEEE Transactions on, vol. 34, no. 3, pp. 860–876, Jul 1998.